Chinese Chemical Letters 34 (2023) 108275

Contents lists available at ScienceDirect

Chinese Chemical Letters

journal homepage: www.elsevier.com/locate/cclet

# Surface charge property governing co-transport of illite colloids and Eu(III) in saturated porous media

Xiaoyan Wei[a,b,c], Duoqiang Pan[a,c,*], Qi Tan[c], Xinyi Shi[c], Junjun Hou[c], Qingfeng Tang[c], Zhen Xu[c], Wangsuo Wu[a,c], Bin Ma[b]

[a] Frontiers Science Center for Rare Isotopes, Lanzhou University, Lanzhou 730000, China
[b] Laboratory for Waste Management, Paul Scherrer Institut (PSI), CH-5232 Villigen PSI, Switzerland
[c] School of Nuclear Science and Technology, Lanzhou University, Lanzhou 730000, China

ARTICLE INFO

*Article history:*
Received 12 November 2022
Revised 31 January 2023
Accepted 27 February 2023
Available online 4 March 2023

*Keywords:*
Illite colloids
Eu(III)
Co-transport
Release
Charge property

ABSTRACT

The transport of colloids and radionuclides is sophisticated because of the variety of charge properties between colloidal particles and host subsurface media, which causes great difficulty in establishing a reliable model of radionuclides migration by taking the colloid phase into consideration. In this work, the co-transport of illite colloids (IC) and Eu(III) in the quartz sand and iron-coated sand porous media was investigated by column experiments to address the predominant mechanism of charge properties on co-transport. Results showed that Eu(III) transport was driven by the illite colloids and electrostatic interaction was critical in governing the co-transport patterns. The promotion of Eu(III) transport by IC was attenuated in the iron-coated sand systems; more IC-Eu(III) complexes were retained uniformly in the column. The pore throat shrinkage caused by electrostatic attachment between aggregated IC and iron oxides exacerbated the physical straining and size exclusion effect of IC-Eu(III) complexes. An aggravated irreversible retention of IC-Eu(III) was detected in iron-coated sand column due to the electrostatic attraction of IC-Eu(III) to host media. The findings are essential for improving the understanding on the potential transport, retention and release risk of colloids associated radionuclides, and imply that the positively charged permeable reactive barrier is an effective strategy to reduce the transport risk of colloid associated radionuclides.



Radionuclides with high radiotoxicity and long half-life originating from nuclear industry activities would have high possibility to intrude into the soil and aquatic environments [1,2]. It was expected that radionuclides can be effectively immobilized by a variety of clay minerals in the geosphere due to their high sorption affinity [3–5]. However, recent studies revealed that radionuclides in the aqueous environment could be detected in aquifers thousands of meters away from the pollution source due to the formation of colloidal particles [6]. The continuous erosion of clay minerals by water can generate a large number of mineral colloids that stably suspend in aqueous solution and efficiently associate with contaminants due to its large specific surface area and high reaction energy [6–8]. Therefore, the colloid-facilitated transport of radionuclides (including radioactive intrinsic colloids or pseudo-colloids) is an ongoing concern in environmental research [9–12].

The transport of radionuclides could be facilitated by the mineral colloids due to the carrying effect of colloids [13–16]. The ability of facilitating radionuclides transport by colloids is strongly correlated to the dispersion stability and mobility ability of colloidal particles [17–19], which are sensitive to the chemical conditions of bulk solution (*e.g.*, pH, ionic strength and colloid concentration) [20–23]. Furthermore, the mobility of colloidal particles is governed by the interaction with host porous media in subsurface environment [24–26]. In the natural environment, the surface charge properties between colloids and host media are diverse due to the difference of mineral composition. In addition, the widespread oxides of iron, aluminum and manganese that have positively charged surfaces are often attached on the negative surface of mineral media and thus alter the surface charge property of soil matrix [27–29].

Recent studies have reported that the surface geochemical heterogeneity of media can affect colloids deposition due to the effects of electrostatic attraction and complexation [27–31]. The mobilization of clay colloids was promoted with the increase of electrostatic repulsion at low ionic strength, high pH, or cladding by

* Corresponding author.
*E-mail address:* panduoqiang@lzu.edu.cn (D. Pan).

https://doi.org/10.1016/j.cclet.2023.108275
1001-8417/

humic substances [32–34]. However, for the opposite charge property of media and colloids, the entrapped colloids by the electrostatic attraction may aggravate the pore shrinkage and pore clogging at the extremely small critical diameter ratio. Furthermore, the electrostatic attachment due to opposite charge and the colloidal coagulation induced by changes in chemical conditions displayed synergistic effects on weakening colloids-driven transport, which complicated the transport behavior and mechanism of radionuclides in the groundwater. It has been reported that the chemical perturbation (*i.e.*, ionic strength reduction and cation exchange) significantly induced the release of retained colloidal cluster from porous column [33–38]. However, when the charge between colloids and media is opposite, the retention and release mechanism of colloids and carried radionuclides were rather complex. Apart from the thickness change of electrical double layer, the electrostatic interaction and complexation may play important roles in influencing the transport and release of colloids and the carried radionuclides. Fundamental knowledge on transport pattern in opposite charge system is required for the reliable model of colloids-driven transport of radionuclides; however, the related mechanism particularly under variable chemical conditions is poorly understood to date, a substantial knowledge gap on charge properties in governing co-transport of colloids and radionuclides still remains.

Illite, as one of the most predominant and typical phyllosilicate minerals in the natural environment, displays appreciable affinity to radionuclides. Both illite colloid and quartz sand mainly display negative surface charge [33,39] and act as the negatively charged system; however, with the adhesion of the positively charged surface of iron oxides, the opposite charge properties would lead to electrostatic interaction between the colloids and host media. And Eu(III) is typically investigated as a chemical analogue of trivalent lanthanides and long-lived radiotoxic actinides owing to the similarity of its physiochemical properties [40]. In this work, the colloid-driven transport and release of Eu(III) in the quartz sand and iron-coated sand porous systems were investigated by column experiments under chemical conditions varying in pH, electrolyte concentration and Eu(III) concentration. The aim of this work is (1) to reveal the role of charge properties between colloid surface and host media in the co-transport and release of IC and Eu(III); (2) to provide a reliable reference for the risk assessment of radionuclides migration in the subsurface environment.

The illite mineral purchased from Jinyuan Mineral Co. (Hebei province, China) was converted into Na-illite [41]. The illite colloid suspension was prepared by dispersing the Na-illite powder in deionized water (m/v = 3 g/L), and then centrifuged at 8000 rpm for 20 min. The detailed preparation and characterization were illustrated in Section S1 (Supporting information) and our previous work [33]. Eu(III) stock solution was prepared from $Eu_2O_3$ (purity, 99.99%, Beijing J&K Scientific Co., Ltd.). All other analytical grade reagents (NaCl (≥99.5%, Tianjin Kemiou Chemical Reagent Co., Ltd.), NaOH (≥96.0%, Damao Chemical Reagent Factory), HCl (Inner Mongolia Huaao Chemical Co., Ltd.) and $Fe(NO_3)_3$ (≥98.5%, Tianjin Kemiou Chemical Reagent Co., Ltd.)) were used without further purification.

Quartz sand (purity > 99.9%) with a homogenized size fraction of 60–80 mesh (420–180 μm) was purified and used as the negatively charged media. In order to examine the role of positive surface charge, the iron-coated sand was prepared as described in literatures [30,31]. Briefly, the quartz sand was coated by the $Fe(OH)_3$, calcined at 105 °C for 72 h, then washed with acid, alkali and deionized water to remove excess ions (as described in Section S2 in Supporting information). The surface morphology and iron content of the quartz sand and iron-coated sand were investigated by scanning electron microscopy and energy dispersive X-ray spectroscopy (SEM-EDX, JSMe6701F, JEOL, Japan). Both images and EDX spectra were shown in Fig. S1 (Supporting information), which indicated that the high iron content of the media surface after the iron oxide coating, and the iron oxide coating did not cause notably discrepancy in the surface roughness of the media.

Transport and release experiments were performed in glass chromatography columns packed with quartz sand or iron-coated sand, respectively. The column was wet-packed with clean sand, a nylon membrane was placed at each end of the column to hold the sand and distribute water flow, the parameters of the packed column were listed in Table S1 (Supporting information). The influent was injected with the direction from bottom to top, and the effluent were collected by a fraction collector at set intervals in 10 mL polyethylene tubes. The release experiments were conducted by eluting with decreasing electrolytes concentration and followed by deionized water and the release experimental conditions were listed in Table 1. The Section S3 (Supporting information) shows the procedures of transport and release experiments.

The Derjaguin, Landau, Verwey and Overbeek (DLVO) theory was applied to predict the interaction of IC-IC and IC-media by calculating the interaction energy as the sum of Lifshitz-van der Waals and stern double layer interactions between IC-IC or IC-media (detailed calculations in Section S4 in Supporting information). The convection-dispersion equation (CDE) with two-site kinetic retention sites was employed to simulate the breakthrough curves of IC and Eu(III) by using the Hydrus-1D and Stanmod software [13,42]. The mathematical model was given in the Section S5 (Supporting information) and the fitting results of tracer were listed in Fig. S2 and Table S2 (Supporting information).

The transport behaviors of Eu(III) were synchronous with colloids and highly dependent on the transport of IC under ambient conditions (Figs. 1 and 2), implying that the mobile colloids governed Eu(III) transport by acting as an efficient carrier. However, compared to the bromide ($Br^-$) tracer breakthrough curves that are almost indistinguishable in the two media (Fig. S2), the breakthrough of IC and Eu(III) was discernibly retarded in iron-coated sand compared with that in quartz sand porous media under the favorable conditions of colloid dispersion. In addition, the exacerbated retention of both IC and Eu(III) was observed at the unfavorable transport conditions in iron-coated sand media in comparison with the negatively charged system, which elucidated that the co-transport behaviors were more sensitive with the fluctuation of counterion concentration in the positively charged media. The electrostatic interaction and the aquatic chemical condition contributed synergistically to the colloids-driven transport of Eu(III).

The breakthrough curves of IC and Eu(III) at various pH values through the quartz sand and iron-coated sand column were plotted in Fig. 1. The Eu(III) transport was significantly facilitated by IC within the concerned pH range compared with the individual transport of Eu(III). The presence of mobile IC greatly promoted the transport ability of Eu(III), and thus increased its leakage risk to biosphere. Due to the prominent Eu(III) sorption ability and transport ability of IC, Eu(III) preferred attaching to mobile IC and transporting simultaneously with IC as a passenger (Fig. S3 in Supporting information). According to the column parameters, there is no difference in the porosity and pore volume (PV) of the iron sand column and the Q-column (Table S1), and thus the size exclusion effect caused by the two media should be the same. However, the significant retardation occurred in the iron-coated sand column even for the dispersed colloids at pH 6, the breakthrough PV of Eu(III)-IC hybrid were 1.0 and 2.1 in the quartz sand and iron-coated sand, respectively (Figs. 1a and c). The effluent mass recovery rate ($M_{eff}$) of Eu(III) in the presence of colloids were 100% and 87% for the quartz sand and iron-coated sand systems at pH 4 (Table S3 in Supporting information), which implied not only that the Eu(III) transport was driven by colloids, but also the electrostatic attraction inhibited the transport ofcolloid-carried

**Table 1**
Detailed setup of column release experiments in saturated porous media.

| Experiment | Media | Breakthrough phase | pH | Phase 1 | | Phase 2 |
|---|---|---|---|---|---|---|
| Exp. 1 | Quartz sand | IC + 5 μmol/L Eu(III) + 7 mmol/L NaCl | 5.0 | 7 mmol/L NaCl | 1 mmol/L NaCl | DI water |
| Exp. 2 | Iron-coated sand | IC + 5 μmol/L Eu(III) + 7 mmol/L NaCl | 5.0 | 7 mmol/L NaCl | 1 mmol/L NaCl | DI water |
| Exp. 3 | Quartz sand | IC + 10 μmol/L Eu(III) + 7 mmol/L NaCl | 5.0 | 7 mmol/L NaCl | 1 mmol/L NaCl | DI water |
| Exp. 4 | Iron-coated sand | IC + 10 μmol/L Eu(III) + 7 mmol/L NaCl | 5.0 | 7 mmol/L NaCl | 1 mmol/L NaCl | DI water |
| Exp. 5 | Quartz sand | IC + 13 μmol/L Eu(III) + 1 mmol/L NaCl | 5.0 | 1 mmol/L NaCl | | DI water |
| Exp. 6 | Iron-coated sand | IC + 13 μmol/L Eu(III) + 1 mmol/L NaCl | 5.0 | 1 mmol/L NaCl | | DI water |

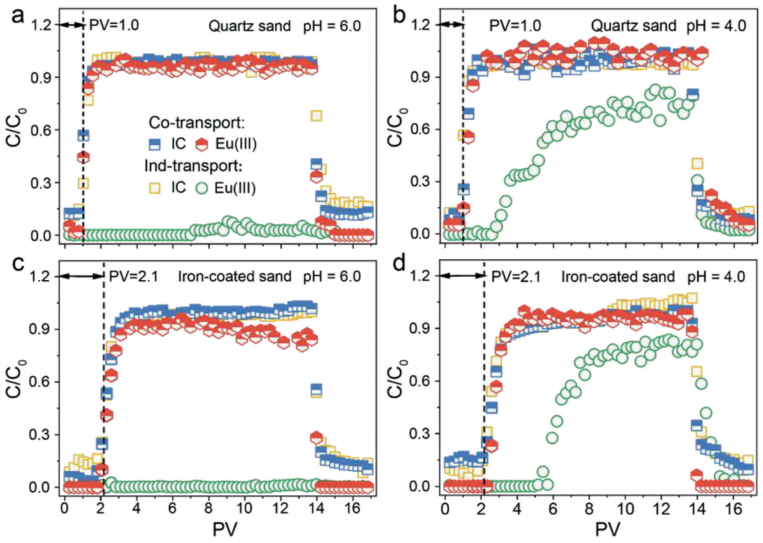


**Fig. 1.** Effect of pH on co-transport of Eu(III) and IC in (a, b) saturated quartz sand and (c, d) iron-coated sand columns. $C_{IC} = 50$ mg/L, $C_{Eu(III)} = 5$ μmol/L, $C_{NaCl} = 1$ mmol/L, $T = 25$ °C.

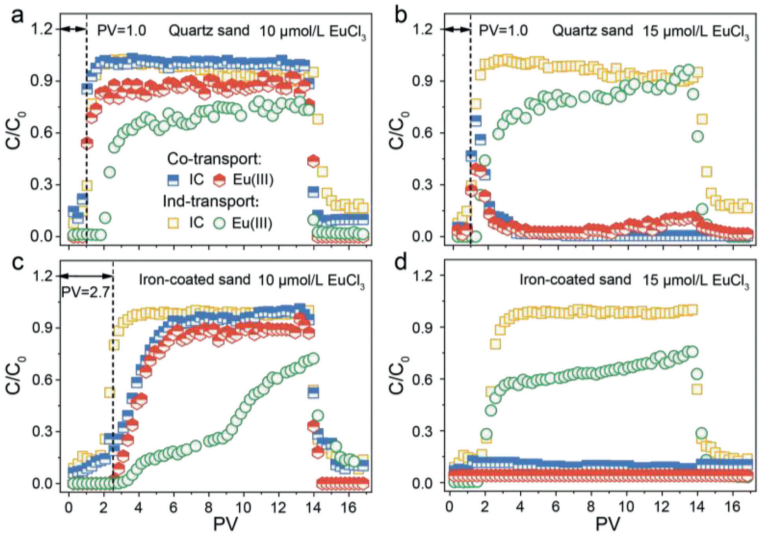


**Fig. 2.** Effect of Eu(III) concentration on co-transport of Eu(III) and IC in (a, b) saturated quartz sand and (c, d) iron-coated sand columns. $C_{NaCl} = 1$ mmol/L, $C_{IC} = 50$ mg/L, pH = 5.0, $T = 25$ °C.

Eu(III). Due to the cladding of iron oxides, the apparent zeta potential of iron-coated sand was less negative compared with that of quartz sand (Fig. S4 in Supporting information), which was responsible for the increased IC retention in the iron-coated sand system. The positively charged iron oxide surface tended to bind with the negatively charged surface of illite colloid particles and led to the strong retention of IC-Eu(III) hybrid, which was consistent with the observation that positively charged packing media showed higher affinity for negatively charged biochar nanoparticles [9,43].

In addition, the discernible retardation was observed during the individual transport of Eu(III) and IC in the iron-coated sand. According to the fitting parameters of two-sites kinetic attachment/detachment model and two-sites nonequilibrium model, the maximum solid-phase retention capacity on site 2 ($S_{max2}$) of colloids (Table 2) and the retardation factor ($R_f$) of Eu(III) (Table 3) in iron-coated sand were accordingly larger than that in quartz sand, which confirmed the enhanced retention of IC and Eu(III) caused by the strong interaction of the iron-coated sand with IC and

**Table 2**
The transport parameters of IC and IC-Eu(III) fitted with the two-site kinetic retention model using HYDRUS-1D program.

| Media | System | $C_{Eu(III)}$ (μmol/L) | $C_{NaCl}$ (mmol/L) | pH | $k_1$ [a] ($min^{-1}$) | $k_{1d}$ [b] ($min^{-1}$) | $S_{max2}$ [c] ($(N_t/N_0)g^{-1}$ sand) | $k_2$ [d] ($min^{-1}$) | $R^2$ [e] |
|---|---|---|---|---|---|---|---|---|---|
| Quartz sand | IC | 0 | 1 | 4.0 | 0.61 | 0.64 | 0.35 | $4.5 \times 10^{-3}$ | 0.97 |
| | | 0 | 1 | 5.0 | 0.69 | 0.50 | 0.50 | $1.7 \times 10^{-2}$ | 0.96 |
| | | 0 | 1 | 6.0 | 0.49 | 0.41 | 0.36 | $1.4 \times 10^{-5}$ | 0.98 |
| | | 0 | 7 | 5.0 | 0.06 | 0.00 | 0.95 | $5.6 \times 10^{-1}$ | 0.95 |
| | IC-Eu(III) | 5 | 1 | 4.0 | 0.61 | 0.63 | 0.42 | $3.3 \times 10^{-3}$ | 0.97 |
| | | 5 | 1 | 5.0 | 1.16 | 1.23 | 0.27 | $1.3 \times 10^{-3}$ | 0.99 |
| | | 5 | 1 | 6.0 | 0.84 | 1.00 | 0.47 | $1.5 \times 10^{-2}$ | 0.99 |
| | | 5 | 7 | 5.0 | 0.43 | 0.44 | 6.24 | $5.5 \times 10^{-1}$ | 0.97 |
| | | 10 | 1 | 5.0 | 0.92 | 1.41 | 0.44 | $5.1 \times 10^{-2}$ | 0.98 |
| Iron-coated sand | IC | 0 | 1 | 4.0 | 0.36 | 0.23 | 0.58 | $4.7 \times 10^{-1}$ | 0.97 |
| | | 0 | 1 | 5.0 | 0.37 | 0.28 | 0.49 | $5.4 \times 10^{-1}$ | 0.98 |
| | | 0 | 1 | 6.0 | 0.39 | 0.30 | 0.47 | $5.4 \times 10^{-1}$ | 0.98 |
| | | 0 | 7 | 5.0 | 0.08 | 0.04 | 5.52 | $8.5 \times 10^{-1}$ | 0.89 |
| | IC -Eu(III) | 5 | 1 | 4.0 | 0.29 | 0.01 | 0.64 | $1.6 \times 10^{-1}$ | 0.89 |
| | | 5 | 1 | 5.0 | 0.33 | 0.12 | 0.63 | $1.0 \times 10^{-1}$ | 0.87 |
| | | 5 | 1 | 6.0 | 0.5 | 0.21 | 0.57 | $5.0 \times 10^{-2}$ | 0.89 |
| | | 10 | 1 | 5.0 | 0.29 | 0.20 | 1.18 | $3.1 \times 10^{-1}$ | 0.99 |

Flow rate = 0.6 mL/min.
[a] First-order retention rate coefficient on site 1.
[b] First-order detachment rate coefficient on site 1.
[c] Maximum solid-phase retention capacity on site 2.
[d] First-order retention rate coefficient on site 2.
[e] *R* Square for regression of observed *vs.* predicted.

**Table 3**
The transport parameters of Eu(III) fitted with non-equilibrium two-site model using CXTFIT.

| Media | $C_{Eu(III)}$ (μmol/L) | $C_{NaCl}$ (mmol/L) | pH | $R_f$ [a] | $\beta$ [b] | $w$ [c] | $R^2$ |
|---|---|---|---|---|---|---|---|
| Quartz sand | 5 | 1 | 4.0 | 50.5 | 0.24 | 0.57 | 0.91 |
| | 5 | 1 | 5.0 | 176.8 | 0.07 | 0.74 | 0.92 |
| | 5 | 1 | 6.0 | 1209 | 0.02 | 3.63 | 0.86 |
| | 5 | 7 | 5.0 | 116.4 | 0.10 | 0.43 | 0.94 |
| | 5 | 10 | 5.0 | 43.1 | 0.24 | 0.42 | 0.93 |
| | 3 | 1 | 5.0 | 165.4 | 0.13 | 1.15 | 0.96 |
| | 10 | 1 | 5.0 | 50.1 | 0.14 | 0.42 | 0.97 |
| | 15 | 1 | 5.0 | 24.7 | 0.27 | 0.27 | 0.94 |
| Iron-coated sand | 5 | 1 | 4.0 | 51.6 | 0.11 | 0.30 | 0.98 |
| | 5 | 1 | 5.0 | 433.5 | 0.06 | 1.66 | 0.84 |
| | 5 | 1 | 6.0 | 5343 | 0.00 | 6.01 | 0.82 |
| | 5 | 7 | 5.0 | 228.7 | 0.08 | 0.47 | 0.97 |
| | 5 | 10 | 5.0 | 63.2 | 0.21 | 0.33 | 0.93 |
| | 15 | 1 | 5.0 | 61.9 | 0.13 | 0.51 | 0.96 |

Flow rate = 0.6 mL/min, darcy flow rate = 2.17 cm/min, dispersion coefficient = 0.0316.
[a] Retardation factor.
[b] Dimensionless the fraction of instantaneous retardation.
[c] Dimensionless mass transfer coefficient.

Eu(III). Note that the Eu(III) alone hardly passed through the column at pH 6; the $R_f$ value of Eu(III) greatly increased with increasing pH. The increasing effect of $R_f$ was stronger in the iron-coated sand column. This was consistent with the observations from the batch sorption experiments, showing that the increased adsorption capacity ($C_s$) of Eu(III) with increasing pH on iron-coated sand was notably higher than that on quartz sand (Fig. S3a) [44]. The parameter $\beta$ representing the fraction of instantaneous retardation decreased with the increase of pH and was smaller in iron-coated sand system than in quartz sand system (Table 3), suggesting that the non-equilibrium adsorption of Eu(III) dominated at high pH and in iron-coated sand media [45]. Hence, the inhibition of the radionuclides transport by metal oxides such as iron oxides was not negligible due to the strong affinity of metal oxides for radionuclides. Despite such strong affinity of Eu(III) to host packing media, the transport behaviors of Eu(III) during the co-transport process were significantly governed by the behavior of IC. The adsorption capacity of Eu(III) on IC was largely higher than that on quartz sand, which even differed in four orders of magnitude (Fig. S3). The strong interaction of IC and Eu(III) resulted in quite stable Eu(III)-colloid particles, which are able to survive under the competition from host media during the co-transport process.

The transport of IC and Eu(III) in quartz sand and iron-coated sand columns under various Eu(III) concentrations was shown in Fig. 2. For the individual transport of Eu(III), as the invariance of adsorption sites in the column, Eu(III) $M_{eff}$ increased continuously with increasing Eu(III) concentration in both media (Table S4 in Supporting information). However, the co-transport $M_{eff}$ of Eu(III) and IC declined simultaneously in both media at the high Eu(III) concentration, even lower than that in individual transport of colloids (Table S3), which implied that the co-transport pattern of Eu(III) depended greatly on the transport behaviors of IC. Previous studies on IC stability have shown that the increase of Eu(III) concentration would not only compress the thickness of the electrical double layer of colloidal particles, but also produce a strong charge shielding effect responsible for the weak electrostatic repulsion between IC particles [39], resulting in the deposition and blocking of Eu(III)-attached colloids in the porous media due to the aggregated IC clusters and the enhanced physic straining [46,47]. Similarly, a large amount of the IC and Eu(III) could be retained at high $Na^+$ concentration (Fig. S5 in Supporting information), indicating that the counter ions had analogous effects in the co-transport. Although a similar diminishing trend for the $M_{eff}$ of colloids and Eu(III) was observed in both quartz sand and iron-coated sand systems with increasing Eu(III) concentration, the decrease of $M_{eff}$ in iron-coated sand was significantly greater than that for quartz sand under all conditions owing to the extra adhesion sites (at 10 μmol/L Eu(III) and 15 μmol/L Eu(III), the $M_{eff}$ values of Eu(III) were 84% and 8% in the quartz sand system, respectively, whereas the values were 70% and 0% in the iron-coated sand). It suggested that the co-transport of IC and Eu(III) in the opposite charge system was more sensitive to the counterions concentration. A plausible explanation was that the negatively charged IC cluster was preferentially retained by positively charged iron oxides, even if the cluster size was not large enough to be filtered and retarded by the pore throat in porous media. The subsequent IC retention caused by electrostatic attraction induced the pore-throat shrinkage of the porous media, which further filtered more IC-Eu(III) hybrid complexes, resulting in more serious blocking. Therefore, synergistic effect of electrostatic interaction and colloids stability in-

duced the stronger retention of IC-Eu(III) complexes in the iron-coated sand system. Overall, whether the transport of Eu(III) was facilitated or retained by IC, its $M_{eff}$ for co-transport was almost identical to that of IC (Table S3). From this point of view, the co-transport behavior of Eu(III) could be predicted by the transport patterns of colloids. Although the retardation effect of iron-coated sand on IC was not dramatic in this work, the transport of IC was indeed affected by the electrostatic interaction between IC and host media even under the favorable conditions of colloid dispersion. Wang *et al.* found that the transport of biochar nanoparticles decreased significantly with increasing surface coverage of iron oxyhydroxide due to the enhanced electrostatic attraction between negatively charged biochar particles and positively charged iron oxyhydroxide [30]. Elmelech *et al.* found that the deposition kinetics of silica colloids were controlled by the density of charge heterogeneity on particle and grain surfaces, the colloid removal efficiency for the given conditions increased from 8% for the bare quartz grains to 95% for the aminosilane-modified quartz grains [48]. Consequently, positively charged coating usually provides favorable retention sites for the negatively charged particles, implying that the positively charged permeable reactive barrier may be served as an effective strategy to control the migration behaviors of mineral colloids associated with radionuclides.

To further decipher the dominant mechanism of IC-Eu(III) co-transport in quartz sand and iron-coated sand, the transport curves of colloids in both individual and co-transport systems were simulated with a two-site kinetic retention model, the corresponding fitting parameters were summarized in Tables 2 and 3. In general, the $k_1$ (attachment rate on site 1) and $k_{1d}$ (detachment rate on site 1) of IC on the grain surface were almost equal, indicating that site 1 was unfavorable to the deposition of colloids. Nevertheless, the $k_1$ and $k_{1d}$ in quartz sand column were higher than those in iron-coated sand column. The proportion of reversible deposition sites in quartz sand system was higher in comparison with the iron-coated sand system, which was consistent with the stronger retention in the iron-coated sand [49,50]. The $k_2$ (attachment rate on site 2) and $S_{max2}$ increased with increasing $Na^+$ and Eu(III) concentrations; the $S_{max2}$ for co-transport was much larger than that of individual transport at the same condition, suggesting Eu(III) with larger ion potential displayed a much larger influence on IC retention than $Na^+$, even though its concentration was much lower. The colloid coagulation caused by the bridging cations ($Z \geq 2$) is an undeniable factor to retard the colloid transport [42,51,52]. Similar to the enhanced colloid aggregation and the retention due to the cation bridging of $Ca^{2+}$ [51], Eu(III) was liable to cause the formation of IC cluster by acting as a bridge. After, the IC-Eu(III) hybrid readily attached to grain surface and resulted in more IC retention in column. Therefore, the bridging effect might be responsible for the hysteresis of co-breakthrough rate compared with the individual breakthrough rate of IC and Eu(III). However, the strong irreversible adhesion of IC in iron-coated sand resulted in a higher $k_2$ in opposite charged system. The iron oxide was vital for the interaction between colloids and grains, which led to the significant retention of IC-Eu(III) hybrid in iron-coated sand.

Moreover, the effect of ionic strength on colloids blocking could be determined by the shape of breakthrough curves [53,54]. The effluent concentration of Eu(III) and IC transited from leveled off (normal shape) to reduction (ripening shape) with increasing $Na^+$ or Eu(III) concentrations in quartz sand (Figs. 2a and b). However, the effluent concentration transition from leveled off to slightly raised (blocking shape) was detected when host media was switched to iron-coated sand (Figs. 2a and c), which indicated that the deposition rates of colloids in co-transport system were different from the charge characteristic of host media [55,56]. The blocking effect derived from rapid filling or blocking of available retention sites often tends to result in a decrease of colloid retention coefficient and an increase in colloid transport, while the ripening effects caused by enhanced aggregation and surface straining are prone to the gradually increased deposition rate [51]. Therefore, the robust colloids stability and weak interaction with pure quartz might account for the normal breakthrough curves in quartz sand column under the low ionic strength. In contrast, the iron oxide cladding provided strong affinity for the stably dispersed IC, the preferential attachment of IC to iron-coated sand caused the decrease of deposition rate, and then the increased breakthrough rate. Note that the deposition rate of IC increased with the augments of injection volume of influent at high Eu(III) and $Na^+$ concentration, which was caused by the strong physical straining and coagulation of IC under such colloid aggregation conditions, the pore shrinkage further aggravated the retention of IC and its carried Eu(III) [55].

The retarded Eu(III) has potential to be released again and increases its leakage risk when condition perturbation occurs. The effect of chemical perturbation on the release of retarded colloids and Eu(III) from the column was shown in Fig. 3. The release peaks of IC and Eu(III) could be observed during the eluting phase, the elution mass recovery rate ($M_{elu}$) increased gradually with the diminishing $Na^+$ concentration of eluent. However, the elution profiles of colloids and Eu(III) were different in quartz sand column and iron-coated sand column when eluting with the same procedure, suggesting different mechanisms and factors prevailing in these systems. For Exp. 1 and Exp. 2 (Figs. 3a and b), the release peaks emerged when eluting with diluted NaCl solution and DI water (Phase 1 and Phase 2). The relatively sharp release peak appeared in the Phase 1 for the iron-coated sand system, which indicated that part of the colloids and Eu(III) was trapped in the secondly minimum. The introduction of low ionic strength eluent resulted in the expansion of colloid double layer and the shallow of secondary minimum [57]. For the Exp. 3 to Exp. 6, subtle release was observed in Phase 1 by eluting with the diluted NaCl solution; however, the flushing with DI water induced great release of IC and Eu(III). The injection of deionized water eliminated the secondary energy minima, the IC-Eu(III) hybrid was released from the secondly minimum. Nonetheless, it should be noted that a large amount of IC and Eu(III) was still retained in the column after flushing with DI water, the retention in iron-coated sand system was higher than that in quartz sand system. For quartz sand, the retain rate ($M_{ret}$) of IC and Eu(III) in column were ~10%, 22%, 27% and 33%, 55%, 30% for Exp. 1, Exp. 3 and Exp. 5, respectively; for iron-coated sand, the $M_{ret}$ of IC and Eu(III) were ~24%, 30%, 33% and 47%, 58%, 53% for Exp. 2, Exp. 4 and Exp. 6 (Table S5 in Supporting information), respectively. Hence, the retention of IC-Eu(III) hybrid was probably due to the contribution from the primary energy minima [31] or at the straining sites such as pore throats, grain-to-grain contacts, and flow stagnation zones [58]. Contrarily, for the individual IC transport in quartz sand, the retained IC was almost completely released and only 2% of IC was detained in column after eluting (Fig. S6 and Table S5 in Supporting information). DLVO calculations suggested that the strong repulsive energy barrier between IC and media was more conducive to IC being trapped at the secondary minimum (Fig. 4), resulting in the reversibility retention for the individual transport of IC. However, it became apparent that the irreversibility retention in positively charged media was stronger than that in negatively charged media ascribed to the lower energy barrier in iron-coated sand system. The retained IC in the iron-coated sand system could not be released completely; its retention profile showed that the retained IC after elution was evenly distributed in the column, implying that the electrostatic interaction with iron oxide played important role in the IC retention (Fig. S6).

In addition, the retention profiles of IC-Eu(III) remained in exponential form after the elution in quartz sand media, while in

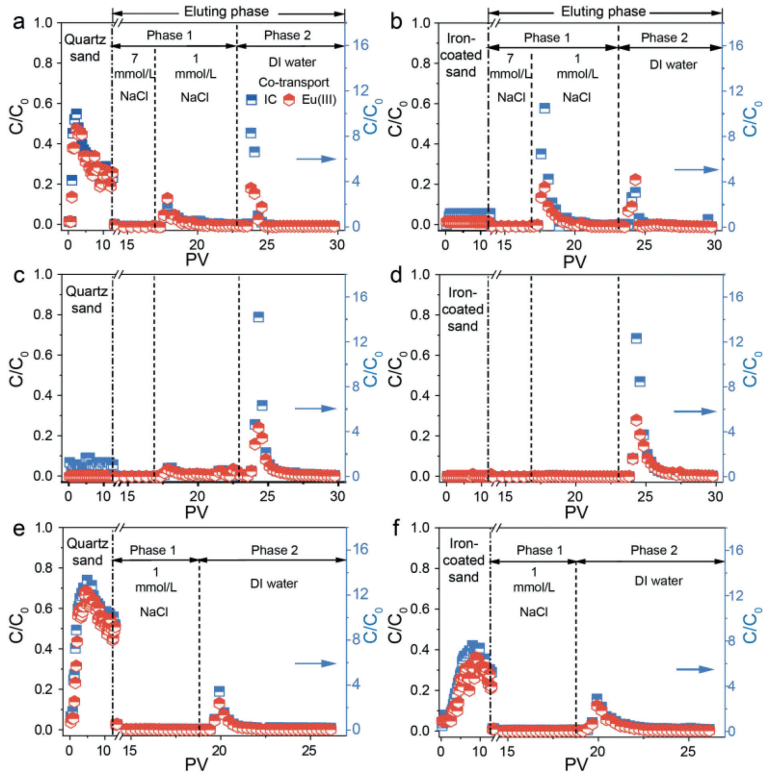


**Fig. 3.** Retention and release of Eu(III) and IC in (a, c, e) saturated quartz sand and (b, d, f) iron-coated sand columns. (a), (b), (c), (d), (e) and (f) are Exp. 1, Exp. 2, Exp. 3, Exp. 4, Exp. 5, and Exp. 6 (detailed conditions are shown in Table 1), respectively, Phase 1 was the elution phase with NaCl, Phase 2 was the elution phase with DI water, the transport phase corresponds to the left ordinate, and the eluting phase corresponds to the right ordinate. (a, b) $C_{Eu(III)} = 5$ μmol/L, $C_{NaCl} = 7$ mmol/L; (c, d) $C_{Eu(III)} = 10$ μmol/L, $C_{NaCl} = 7$ mmol/L; (e, f) $C_{Eu(III)} = 13$ μmol/L, $C_{NaCl} = 1$ mmol/L. $C_{IC} = 50$ mg/L, pH = 5.0, $T = 25$ °C.

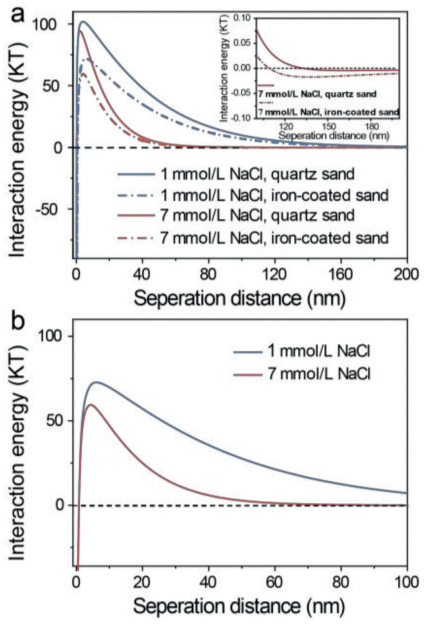


**Fig. 4.** Calculated DLVO interaction energy of colloidal particles and media as a function of separation distance at different NaCl concentrations. (a) IC-media, (b) IC-IC.

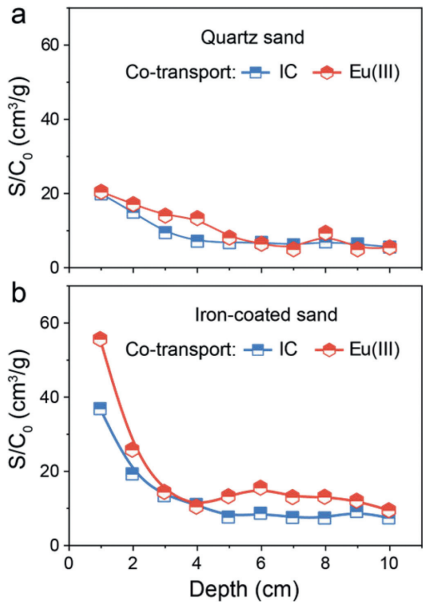


**Fig. 5.** Retention profiles of IC and Eu(III) after completion of release experiments in (a) saturated quartz sand and (b) iron-coated sand columns. $C_{IC} = 50$ mg/L, $C_{Eu(III)} = 13$ μmol/L, $C_{NaCl} = 1$ mmol/L, pH = 5.0, $T = 25$ °C.

hyper-exponential form in the iron-coated sand media (Fig. 5). Therefore, the retention mechanism of IC-Eu(III) hybrid was in response to both electrostatic interaction and chemical conditions. More IC-Eu(III) hybrid was trapped at the primary minimum in the iron-coated sand media [59]. The coating iron oxide acted as the binder for the irreversible retention of colloid, and thus accounted for the pronounced physical straining and ripening effect. In addition, the bridge effect of Eu(III) could not be neglected for the irreversible retention of IC-Eu(III) hybrid. The decreased $C_{Na}/C_{Eu}$ was responsible for the increased ratio of irreversible retention. In Exp. 1 and Exp. 2, $Na^+$ played a dominant role in the deposition of IC-

Eu(III) due to the double layer compression of IC by high $Na^+$ concentration, and thus the injection of low ionic strength eluent expanded the double layer and resulted in re-entrainment of IC and Eu(III). Nevertheless, with the decrease of $C_{Na}/C_{Eu}$ (at high Eu(III) concentration), IC-Eu(III)-IC bridging was the dominant mechanism of colloids deposition. The lowered $Na^+$ concentration in the eluent could not liberate the retained IC and Eu(III). He *et al.* revealed that the retained carboxylated graphene was not released by eluting with deionized water [57]; however, a dramatic release occurred when the $Ca^{2+}$ bridging effect was disrupted by replacing $Ca^{2+}$ with $Na^+$. Therefore, the re-entrainment peaks observed in the Phase 3 for all experiments were related to the cation exchange between Eu(III) and $Na^+$ during the Phase 1 and the expansion of colloid double layer in Phase 2.

This research highlighted that the charge properties of media have a non-negligible effect on mitigating the transport risk of colloids associated radionuclides. The positively charged media induced the attenuating effects of colloid-facilitated Eu(III) transport due to the electrostatic interaction between IC and iron oxides under the colloids dispersion favorable conditions. Additionally, the pores shrink governed by electrostatic interaction of IC and iron oxides exacerbated the physical straining and size exclusion effect of IC-Eu(III) complexes, resulting in the reinforcing effect of IC-Eu(III) complexes retention under the colloids dispersion unfavorable conditions. The retention of IC and IC-Eu(III) in negatively charged media was partly reversible in view of the chemical conditions perturbation, it could be released by ions exchange with the low $Na^+$ eluents and eluting with deionized water. Hence, when glacial water, rain or snow melting invaded into the environmental media which may induce the release and re-transport risk of the deposited and retained colloids and radionuclides. Nonetheless, the retained IC-Eu(III) complexes were weakly released in iron-coated sand system induced by the indestructibility of electrostatic interactions and the irreversibility of physical straining results from pore throat shrinkage. Therefore, as expected from the strong inhibitory and retention irreversibility of charge heterogeneity on colloid-driven radionuclides transport, the positively charged permeable reactive barrier may be an effective strategy to reduce the transport risk of colloid associated radionuclides.

## Declaration of competing interest

The authors declare that there are no competing interests to declare.

## Acknowledgments

This work was supported by the National Natural Science Foundation of China (Nos. 22176077, 22006060), the Fundamental Research Funds for the Central Universities (No. lzujbky-2022-sp04), and Science and Technology Program of Gansu Province, China (No. 20JR10RA615).

## Supplementary materials

Supplementary material associated with this article can be found, in the online version, at doi:10.1016/j.cclet.2023.108275.

## References

[1] H. Ji, Y. Zhu, J. Duan, W. Liu, D. Zhao, Chin. Chem. Lett. 30 (2019) 2163–2168.
[2] E.L. Tran, N. Teutsch, O. Klein-BenDavid, N. Weisbrod, Sci. Total Environ. 643 (2018) 260–269.
[3] T. Yu, W. Wu, Q. Fan, Chin. Chem. Lett. 23 (2012) 1189–1192.
[4] T. Missana, M. Garciá-Gutiérrez, Ú. Alonso, Appl. Clay Sci. 26 (2004) 137–150.
[5] Z. Chen, S. Wang, H. Hou, et al., Chin. Chem. Lett. 33 (2022) 3405–3412.
[6] R. Kretzschmar, M. Borkovec, D. Grolimund, M. Elimelech, Adv. Agron. 66 (1999) 121–193.
[7] S. Czigány, M. Flury, J.B. Harsh, Environ. Sci. Technol. 39 (2005) 1506–1512.
[8] G.E. Walshe, L. Pang, M. Flury, M.E. Close, M. Flintoft, Water Res. 44 (2010) 1255–1269.
[9] M. Chen, X. Chen, X.Y. Xu, et al., J. Hazard. Mater. 440 (2022) 129691.
[10] C. Chen, K. Zhao, J. Shang, et al., Environ. Pollut. 240 (2018) 219–226.
[11] A.P. Novikov, S.N. Kalmykov, S. Utsunomiya, et al., Science 314 (2006) 638–641.
[12] A.B. Kersting, D.W. Efurd, D.L. Finnegan, et al., Nature 397 (1999) 56–59.
[13] M. Chen, X. Tao, D. Wang, et al., Sci. Total Environ. 684 (2019) 265–275.
[14] S. Chotpantarat, N. Kiatvarangkul, Water Res. 146 (2018) 216–231.
[15] D. Wang, M. Paradelo, S.A. Bradford, et al., Water Res. 45 (2011) 5905–5915.
[16] A. Wolfsberg, Z. Dai, L. Zhu, et al., Environ. Sci. Technol. 51 (2017) 5582–5590.
[17] M. Ge, D. Wang, J. Yang, et al., Water Res. 147 (2018) 350–361.
[18] Z. Xu, D.Q. Pan, Q.F. Tang, et al., Environ. Pollut. 298 (2022) 118842.
[19] J. Yang, Z. Zhang, Z. Chen, et al., Sci. Total Environ. 688 (2019) 450–461.
[20] Y. Wang, W. Zhang, J. Shang, C. Shen, S.D. Joseph, Environ. Sci. Technol. 53 (2019) 8136–8146.
[21] J. Won, S.E. Burns, Environ. Sci. Technol. 52 (2018) 2735–2741.
[22] Z. Xu, Y.L. Sun, Z.W. Niu, et al., Appl. Clay Sci. 184 (2020) 105393.
[23] K. Zhao, C. Chen, T. Cheng, J. Shang, Environ. Pollut. 247 (2019) 668–677.
[24] C. Chen, J. Shang, X. Zheng, et al., Environ. Pollut. 236 (2018) 168–176.
[25] Y. Su, B. Gao, L. Mao, Water Res. 115 (2017) 84–93.
[26] M. Wang, B. Gao, D. Tang, C. Yu, Environ. Pollut. 235 (2018) 350–357.
[27] P.R. Johnson, N. Sun, M. Elimelech, Environ. Sci. Technol. 30 (1996) 3284–3293.
[28] J.N. Ryan, P.M. Gschwend, Geochim. Cosmochim. Acta 56 (1992) 1507–1521.
[29] L. Song, P.R. Johnson, M. Elimelech, Environ. Sci. Technol. 28 (1994) 1164–1171.
[30] D. Wang, W. Zhang, D. Zhou, Environ. Sci. Technol. 47 (2013) 5154–5161.
[31] D. Wang, C. Shen, Y. Jin, et al., Sci. Total Environ. 579 (2017) 776–785.
[32] S.A. Bradford, H. Kim, J. Environ. Qual. 39 (2010) 2040–2046.
[33] X.Y. Wei, D.Q. Pan, Z. Xu, et al., Sci. Total Environ. 768 (2021) 144174.
[34] Z. Xu, Z.W. Niu, D.Q. Pan, et al., Sci. Total Environ. 793 (2021) 148545.
[35] J. Ali, Y. Li, E. Shang, et al., Chin. Chem. Lett. 34 (2023) 107327.
[36] S.A. Bradford, S. Torkzaban, H.J. Kim, J.R. Simunek, Water Resour. Res. 48 (2012) W09509.
[37] Y. He, Y. Liu, F. Guo, et al., Chin. Chem. Lett. 31 (2020) 1625–1629.
[38] Y. Zhang, X. Su, N.F.Y. Tam, et al., Chin. Chem. Lett. 33 (2022) 5213–5217.
[39] W.P. Johnson, A. Rasmuson, E. Pazmino, M. Hilpert, Environ. Sci. Technol. 52 (2018) 7230–7239.
[40] M. Zheng, H. Ji, J. Duan, et al., Environ. Sci. Ecotechnol. 2 (2020) 100031.
[41] D. Pan, Q. Fan, P. Li, S Liu, W. Wu, Chem. Eng. J. 172 (2011) 898–905.
[42] S. Torkzaban, J. Wan, T.K. Tokunaga, S.A. Bradford, J. Contam. Hydrol. 136-137 (2012) 86–95.
[43] N. Xu, X. Cheng, D. Wang, et al., Water Res. 146 (2018) 264–274.
[44] Z. Lu, Z. Hao, J. Wang, L. Chen, J. Ind. Eng. Chem. 34 (2016) 374–381.
[45] H.N. Wang, J.C. Liu, J.N. Yao, et al., Water Res. 186 (2020) 116325.
[46] M. Auset, A.A. Keller, Water Resour. Res. 42 (2006) W12S02.
[47] S. Xu, B. Gao, J.E. Saiers, Water Resour. Res. 42 (2006) W12S16.
[48] M. Elimelech, M. Nagai, C.H. Ko, J.N. Ryan, Environ. Sci. Technol. 34 (2000) 2143–2148.
[49] S.A. Bradford, S.R. Yates, M. Bettahar, J. Simunek, Water Resour. Res. 38 (2002) 1327.
[50] S. Dong, X. Shi, B. Gao, et al., Environ. Sci. Technol. 50 (2016) 10397–10405.
[51] Y. Liang, S.A. Bradford, J. Simunek, E. Klumpp, Sci. Total Environ. 656 (2019) 70–79.
[52] Y. Zhang, Y. Chen, P. Westerhoff, J.C. Crittenden, Environ. Sci. Technol. 42 (2008) 321–325.
[53] J.D. Lanphere, B. Rogers, C. Luth, C.H. Bolster, S.L. Walker, Environ. Eng. Sci. 31 (2014) 350–359.
[54] Y. Sun, B. Gao, S.A. Bradford, et al., Water Res. 68 (2015) 24–33.
[55] G. Chen, X. Liu, C. Su, Environ. Sci. Technol. 46 (2012) 7142–7150.
[56] D. Wang, Y. Jin, D.P. Jaisi, J Contam. Hydrol. 182 (2015) 194–209.
[57] J. He, D. Wang, W. Zhang, D. Zhou, Chemosphere 235 (2019) 643–650.
[58] W.P. Johnson, X.Q. Li, G. Yal, Environ. Sci. Technol. 41 (2007) 1279–1287.
[59] W.J. Sang, V.L. Morales, W. Zhang, et al., Environ. Sci. Technol. 47 (2013) 8256–8264.